Climate Dynamics
https://doi.org/10.1007/s00382-023-07066-1

ORIGINAL ARTICLE

The offshore wind speed changes in China: an insight into CMIP6 model simulation and future projections

Kaiqiang Deng[1,2,3] · Song Yang[1] · Wanlei Liu[1] · Hairong Li[1] · Deliang Chen[4] · Tao Lian[3] · Gangfeng Zhang[5] · Jinlin Zha[6] · Cheng Shen[4]

Received: 22 September 2023 / Accepted: 9 December 2023

Abstract

Offshore wind speed in China plays a key role in affecting air–sea interactions, coastal tides, and wind energy, but its changes in a warming climate and the associated causes remain unclear. Based on the ERA5 reanalysis and the Coupled Model Intercomparison Project Phase 6 (CMIP6) models, this study evaluates the past and future variations of wind speed at 10 m (WS10) over China's offshore seas in summer and winter. The results show that the CMIP6 multi-model mean performs well in simulating the climatological patterns (1981–2010) of WS10 for both seasons. The trends and leading variabilities in WS10 are also reasonably reproduced in the South China Sea (SCS). In the northern SCS, WS10 has strengthened during both seasons in the recent decades. In contrast, in the East China Sea (ECS), WS10 has increased (decreased) during summer (winter). Further attribution analysis suggests that the forcing of greenhouse gasses (aerosols) may make WS10 stronger (weaker) in the two seas and for both seasons, while natural variability tends to slow down (speed up) WS10 in the SCS and ECS during summer (winter). In addition, according to the CMIP6 model projections under various warming scenarios, WS10 is likely to increase over both the northern SCS and the ECS in summer, while WS10 will increase over the northern SCS but decrease over the ECS in winter. Differences in the projected WS10 changes in the ECS during summer and winter are attributed to the projected intensification (weakening) of the East Asian summer (winter) monsoon circulation.

Keywords Offshore wind speed · China · CMIP6 · Simulation · Projection

1 Introduction

Wind speed at 10 m (WS10) is an important meteorological parameter that can greatly affect both the natural environment and human society (Zeng et al. 2019; McVicar et al. 2012; Yu 2007). Over the oceans, WS10 plays a critical role in air–sea interactions by regulating the heat and moisture fluxes, which thus influences oceanic and atmospheric circulations (Drennan et al. 2014; Högström et al. 2013). In nearshore waters, an increase in WS10 can lead to storm surges and sea level rise, posing a significant threat to coastal infrastructure, maritime traffic, and fishermen's safety (Baksh et al. 2018; Dasgupta et al. 2011; Mariotti et al. 2010). In addition, the offshore wind energy has gained importance and developed rapidly in recent years. A 2023 report by the World Forum Offshore Wind showed that 42 new offshore wind farms were commissioned in 2022, of which 29 were installed in China (WFO 2023). Since wind power is proportional to the third power of the near-surface wind speed, even small changes in the near-surface wind

✉ Song Yang
yangsong3@mail.sysu.edu.cn

1 School of Atmospheric Sciences, Sun Yat-sen University, and Southern Marine Science and Engineering Guangdong Laboratory (Zhuhai), Zhuhai, Guangdong, China

2 Key Laboratory of South China Sea Meteorological Disaster Prevention and Mitigation of Hainan Province, Hainan Meteorological Service, Haikou, Hainan, China

3 State Key Laboratory of Satellite Ocean Environment Dynamics, Second Institute of Oceanography, Hangzhou, Zhejiang, China

4 Department of Earth Sciences, University of Gothenburg, Gothenburg, Sweden

5 State Key Laboratory of Earth Surface Processes and Resource Ecology, Beijing Normal University, Beijing, China

6 Department of Atmospheric Sciences, Yunnan University, Kunming, Yunnan, China

Published online: 19 January 2024

conditions can have significant impacts on wind energy production (Carvalho et al. 2021; Pryor et al. 2020; Hdidouan and Staffell 2017; Saidur et al. 2010). Therefore, to mitigate potential risks and maximize benefits, it is of great importance to better understand the past and future changes in the offshore winds and their associated causes.

The coastal waters of China are dominated by the monsoon climate during the boreal summer and winter. Strong southerly and southwesterly winds occur over Southeast Asia, East China, Japan, the Korean Peninsula, and adjacent seas in summer (Chen and Yang 2023; Sun et al. 2022; Lu et al. 2021), while northerly and northeasterly winds prevail along the East Asian coasts and nearshore seas in winter (Miao and Wang 2020; Wang and Chen 2014; Li and Yang 2010). Monsoon circulations are mainly driven by the thermal contrast between land and ocean and are therefore sensitive to global climate change (Chen et al. 2020; Lin et al. 2014; Chen and Sun 2013; Wang and Ding 2006). Recent studies suggest that the East Asian summer monsoon circulation may strengthen in response to future climate warming (Park et al. 2020; Li et al. 2019; He et al. 2019; Chen et al. 2019), while in winter, the Siberian high and East Asian trough are projected to weaken, implying a weaker East Asian winter monsoon circulation in the future (Miao et al. 2020; Gong et al. 2018; Xu et al. 2016).

Previous studies have extensively investigated WS10 changes in China, but most of them focused on land areas. For example, based on in situ observations, Guo et al. (2011) reported a significant weakening of annual and seasonal mean WS10 values in China from 1969–2005, with an average annual trend of − 0.18 m s^{-1} $decade^{-1}$. Li et al. (2022) similarly found a significant decline in WS10 in China during 1979–2019, particularly during 1979–1996, with a rate of decline of − 0.06 and − 0.19 m s^{-1} $decade^{-1}$, respectively. This phenomenon of a long-term decline in WS10 over land is referred to as "terrestrial stilling" (Azorin-Molina et al. 2018; McVicar et al. 2012; Roderick et al. 2007). Other studies based on global atmospheric reanalysis data and model simulations have also found decreasing trends in WS10 over China from the mid-twentieth century (Yu et al. 2019a, b; Zhang et al. 2019). Nevertheless, in recent years, there has been increasing evidence that WS10 has recovered since the 2010s, when a significant increase in WS10 has been recorded over eastern and northern parts of China (Yang et al. 2021; Zha et al. 2021; Zeng et al. 2019).

Previous studies have also assessed the past and future variations of the offshore wind speed in China. For example, Yu et al. (2019a, b) analyzed the offshore wind characteristics and wind energy potential of Bohai Bay in China using 2-year offshore wind data and showed that the main wind direction in Bohai Bay is from the east, with the speed mainly between 4 and 8 m s^{-1}. Wen et al. (2021) investigated the long-term offshore wind energy potential on the south and southeast coast of China based on a 55-year dataset. They found that the Luzon Strait and Taiwan Strait have a higher wind energy potential than other areas and that the long-term trend of wind energy has been largely uniform overall over the past five decades. Zheng et al. (2019) evaluated the future projections of global offshore wind energy resources using the Coupled Model Intercomparison Project Phase (CMIP) data. Their results indicate that the extent of areas with a wind power density of more than 400 W m^{-2} will increase compared to the past. In the future, the effective wind speed and wind power density of more than 200 W m^{-2} will generally increase by 10% in most of the world's oceans. Zhang and Li (2021) further evaluated the projection of future offshore wind energy resources in China using a newly developed downscaling method based on a deep learning network. The results indicate a slight decrease in offshore wind speed and wind power density over the East China Sea (ECS) and an increase in these parameters over the South China Sea (SCS) in the middle and end of the twenty-first century.

Although WS10 trends are known over Chinese land areas, WS10 changes in China's offshore seas and their associated causes remain unclear. Unlike the land areas, where the long-term decline in WS10 could be associated with increased surface roughness, such as the taller trees and greening vegetation due to global warming and the rapid urbanization caused by human activities (Zhang et al. 2022a, b; Zhang and Wang 2020; Zhang et al. 2019; Wever 2012; Vautard et al. 2010), the changes in winds at the sea surface do not appear to be related to the land use and land cover changes. However, the variations in sea surface winds could be directly caused by the non-uniform warming of the sea surface and the resulting surface pressure gradient (Shen et al. 2022; Zhang et al. 2020; Wu et al. 2018). In addition, the ocean–atmosphere coupling oscillations in the tropical and extratropical oceans, such as the North Atlantic Oscillation and the Pacific Decadal Oscillation, may lead to anomalous atmospheric teleconnection patterns that affect the large-scale atmospheric circulation (e.g. the monsoons) and thus the variations and changes of WS10 in the nearshore waters of China in summer and winter (Deng et al. 2021, 2022; Kim et al. 2021; Zeng et al. 2019; Chen et al. 2013).

In addition to in-situ observations and global atmospheric reanalyses, climate models are a good tool to investigate factors relevant to WS10 changes. Wu et al. (2020) and Shen et al. (2022) evaluated the performance of more than twenty models from the CMIP6 in simulating annual and seasonal averages of WS10 on land and found that the ensemble mean of the models was able to reproduce the spatial distribution of WS10 changes in China. In addition, the CMIP6 models appear to have better simulated the climatological pattern of large-scale atmospheric circulation patterns over East Asia compared to the CMIP5 models, which is attributed to

improved simulation of sea surface temperature biases over the Northwest Pacific (Xin et al. 2020). However, whether CMIP6 models can faithfully represent WS10 over China's coastal waters and its changes and variability is not well evaluated, partly due to the lack of reliable observational data over the seas. In recent years, reanalysis products have matured and are increasingly used for climate studies, providing a way to address the problem of lack of observations.

Therefore, this study aims to evaluate the performance of CMIP6 models in reproducing WS10 over China's surrounding seas. Based on the CMIP6 simulations with the historical all forcings and the individual forcings, we also evaluate the relative contributions of anthropogenic forcings and natural variability in affecting the offshore WS10. Finally, we evaluate the future changes in the offshore WS10 based on the CMIP6 projections under various warming scenarios. The remainder of this paper is organized as follows. Section 2 outlines the data and methods used in this study. Sections 3 and 4 present the research results, followed by a summary and discussion in Sect. 5.

2 Data and methods

2.1 Reanalysis data

Reanalysis data have several advantages over station observations, such as broader spatial coverage and consistent temporal resolution, making them particularly useful in ocean regions where ground-based records are limited. Fan et al. (2021a, b) evaluated the performance of five reanalysis products (ERA5, ERA-Interim, MERRA-2, JRA-55, and CFSv2) in representing global WS10 changes and reported that the ERA5 data are closest to observations. Based on buoy observations in the coastal waters of Zhejiang Province, China, Wu et al. (2022) investigated the reliability of three commonly used wind products (CFSv2, ERA5, and Cross-Calibrated Multi-Platform data) in measuring WS10. ERA5 was found to slightly outperform the other wind products over East Asian coastal waters. By analyzing meteorological data from the ocean field experiments, Xu et al. (2022) also reported that the ERA5 products performed better in determining the wind characteristics over the adjacent seas of China. Therefore, this study investigates the variations and changes of WS10 mainly based on the ERA5 reanalysis data (Hersbach et al. 2020; Hersbach and Dee 2016). The ERA5 reanalysis data assimilates in-situ observations and has a horizontal resolution of $0.25° \times 0.25°$ and 137 hybrid levels in the vertical direction for the period from 1979 to the present.

We also analyze atmospheric circulation data to investigate the physical factors contributing to the WS10 changes. The atmospheric datasets we use include geopotential height and three-dimensional velocities at multiple pressure levels. These datasets were all from the ERA5 reanalysis, which can be accessed at https://cds.climate.copernicus.eu/cdsapp#!/search?type=dataset. To facilitate comparison, the ERA5 data were interpolated to a monthly time scale and a horizontal resolution of $1° \times 1°$ for the period from 1979 to 2023. In addition, this study analyzes the fifth version of the NOAA Extended Reconstructed Sea Surface Temperature, covering the period from January 1854 to the present, with a horizontal resolution of $2° \times 2°$ (Huang et al. 2017), downloaded from https://www.ncei.noaa.gov/products/extended-reconstructed-sst.

2.2 CMIP6 datasets

The CMIP6 historical simulation and future projection datasets are analyzed in this study (Eyring et al. 2016). These models were developed to simulate observed variables within the climate system from 1850 to 2014 and to project changes within the climate system beyond 2015. A total of twenty models were utilized in this study (listed in Table 1).

To assess the reliability of the CMIP6 models, we first evaluate their ability to represent the WS10 climatology and trends, as well as the leading mode of WS10 variability, over the nearshore waters of China. To explore the relative contributions of anthropogenic emissions and natural variability, we separately examine the trends and uncertainty of WS10 in each set of CMIP6 simulations containing only greenhouse gas (GHG), only aerosol, and only natural variability. Comparisons between WS10 trends simulated by historical all-forcing and trends simulated by historical individual forcings allow us to quantitatively assess the relative contributions of these factors involved in the WS10 changes.

We further evaluate the future WS10 changes based on CMIP6 projections under four Shared Socioeconomic Pathway (SSP) scenarios: SSP126, SSP245, SSP370, and SSP585. These four scenarios represent a range of GHG emissions from low to high levels. Compared to the representative concentration pathway scenarios used in CMIP5, the SSP scenarios in CMIP6 provide a more comprehensive set of assumptions about the social, technological, cultural, educational, and economic developments expected for the twenty-first century (O'Neill et al. 2016). In addition to the WS10, we also evaluate the changes in precipitation, 2-m air temperature, and sea-level pressure, as well as changes in 3-dimensional wind velocities and geopotential height at multiple pressure levels. All of these simulated and projected CMIP6 datasets are publicly available through the website https://esgf-node.llnl.gov/search/cmip6/.

Table 1 Model name, affiliated institution, and horizontal resolution of the twenty CMIP6 models analyzed in this study

Model name	Institution (Country)	Resolution (km)
ACCESS-CM2	Commonwealth Scientific and Industrial Research Organisation (Australia)	250
ACCESS-ESM1-5		
BCC-CSM2-MR	Beijing Climate Center (China)	100
CAMS-CSM1-0	Chinese Academy of Meteorological Sciences (China)	100
CanESM5	Canadian Centre for Climate Modelling and Analysis (Canada)	500
CanESM5-CanOE		
CESM2-WACCM	National Center for Atmospheric Research (USA)	100
CMCC-CM2-SR5	Euro-Mediterranean Centre for Climate Change (Italy)	100
CNRM-CM6-1	National Center for Meteorological Research (France)	250
CNRM-ESM2-1		
GFDL-ESM4	NOAA's Geophysical Fluid Dynamics Laboratory (USA)	100
INM-CM4-8	Institute for Numerical Mathematics (Russia)	100
INM-CM5-0		
KACE-1-0-G	National Institute of Meteorological Sciences (South Korea)	250
MIROC6	Japan Agency for Marine-Earth Science and Technology (Japan)	250
MIROC-ES2L		
MPI-ESM1-2-LR	Max Planck Institute for Meteorology (Germany)	250
MRI-ESM2-0	Meteorological Research Institute (Japan)	100
NorESM2-LM	Norwegian Climate Centre (Norway)	250
NorESM2-MM		

2.3 Methods

For better comparison and to facilitate the calculation of multi-model ensemble mean, all CMIP6 datasets were interpolated onto a $2° \times 2°$ grid using a bilinear interpolation method (Zhang et al. 2022a, b). The WS10 is calculated as $\sqrt{u^2 + v^2}$, where u and v are the zonal and meridional components of the 10-m winds, respectively. The boreal summer and winter are defined as 3-month means of JJA (June–July–August) and DJF (December–January–February), respectively. Other statistical methods include empirical orthogonal function (EOF) analysis, correlation and regression analysis, and linear trend analysis. For correlation analysis and trend analysis, we use the Student's *t*-test to determine the statistical significance of the results.

This study mainly focuses on the WS10 changes over the nearshore waters of China and in the summer and winter seasons, when the East Asian summer and winter monsoons dominate the regional atmospheric circulations. For simplicity, two monsoon indices are employed to represent the intensity of the East Asian summer and winter monsoons, respectively. For summer, Wang et al. (2008) compared 25 existing indices for the East Asian summer monsoon and recommended a simple index, the inverse Wang and Fan index (here referred to as WFI; Wang and Fan 1999), defined as U850 in (22.5°–32.5° N, 110°–140° E) minus U850 in (5°–15° N, 90°–130° E). This index represents the shear vorticity and is widely used to measure the East Asian and the Northwest Pacific summer monsoon circulation. For winter, the thermal contrast between the Asian continent and the adjacent oceans is the main cause of the East Asian winter monsoon, which can be well represented in the sea-level pressure field (Wang and Chen 2014). Accordingly, the East Asian winter monsoon index (here referred to as WCI) is defined by $(2 \times \mathrm{SLP1}^* - \mathrm{SLP2}^* - \mathrm{SLP3}^*)/2$, where SLP1*, SLP2*, and SLP3* represent the area-averaged sea-level pressure over Siberia (40°–60° N, 70°–120° E), the North Pacific (30°–50° N, 140° E–170° W), and the Maritime Continent (20° S–10° N, 110°–160° E), respectively.

3 Historical simulation of the WS10 changes in summer and winter

3.1 Climatology, trends, and leading variability

Figure 1 shows the WS10 climatological values for summer and winter obtained from the ERA5 reanalysis and the CMIP6 historical simulations. For both seasons, the multi-model ensemble mean accurately simulated the spatial distribution and magnitude of WS10. In summer, both the ERA5 reanalysis and the model simulations show WS10 above $+6.0$ m s^{-1} over the SCS and WS10 between $+3.0$ and $+4.0$ m s^{-1} over the Philippine Sea (Fig. 1a, b). In

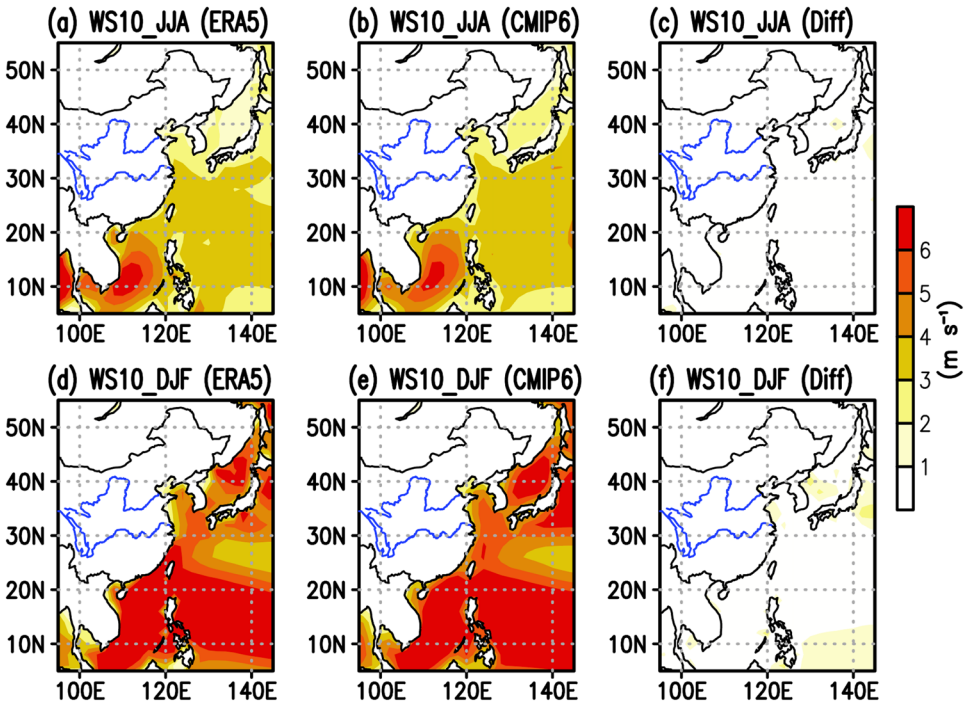

Fig. 1 The WS10 climatology (1981–2010) (unit: m s^{-1}) in summer for **a** ERA5, **b** CMIP6, and **c** the difference between CMIP6 and ERA5. **d**–**f** Similar to **a**–**c** except for winter. The spatial correlations between the ERA5 and CMIP6 patterns are +0.93 in summer and +0.94 in winter

winter, WS10 of more than +6.0 m s^{-1} is observed over most waters, including the SCS, Philippine Sea, ECS, and Sea of Japan (Fig. 1d, e). The differences in WS10 between the CMIP6 ensemble mean and the ERA5 are further shown in Fig. 1c for summer and in Fig. 1f for winter. We see the biases of WS10 climatology are less than 1 m s^{-1} in most ocean surfaces in both seasons, although in winter the CMIP6 WS10 climatology is slightly larger than that in the ERA5. The spatial correlation coefficients between the two WS10 climatological patterns are +0.93 for summer and +0.94 for winter, respectively. This further demonstrates that the CMIP6 multi-model ensemble mean is reliable in simulating the WS10 climatology in summer and winter.

Figure 2 displays the first leading EOF mode (EOF1) of WS10 variability for the ERA5 reanalysis and the CMIP6 model simulations during the two seasons. The WS10 variability refers to the fluctuations and deviations of WS10 from the climatology over a long-term scale. In summer, the EOF1 is characterized by a decrease in WS10 over the southern SCS and an increase in WS10 over the northern SCS (Fig. 2a). As seen from Fig. 2b, the CMIP6 multi-model mean correctly captured the seesawing WS10 variability in the northern and southern SCS areas, but it overestimated the WS10 signals in the ECS. In winter, the EOF1 is featured by a uniform WS10 variability over the coastal waters of East Asia, with increased WS10 over the northern SCS, northern Philippine Sea, and high latitude waters, while a decrease in WS10 occurs only in the tropical western Pacific (Fig. 2d, e). In contrast to summer, where the largest WS10 variations exist in the southern SCS, winter WS10 exhibits strong variability along the entire nearshore seas of East Asia. For both seasons, the EOF1 modes from the reanalysis show much larger interannual variations than the simulated ones (Fig. 2c and f). In addition, the CMIP6 multi-model mean appears to show better performance in simulating the leading pattern of the WS10 variability at lower latitudes than at high latitudes.

Figure 3 further presents the WS10 trends for the ERA5 reanalysis and the CMIP6 model simulations. In summer, the ERA5 reanalysis reveals positive WS10 trends in the nearshore waters along the Chinese coasts (Fig. 3a), indicating enhanced winds over these areas. However, WS10 values over the southern SCS have decreased over the historical period. In general, the CMIP6 multi-model mean has reproduced the spatial patterns of the reanalysis WS10 trends to some extent during summer, with enhanced WS10 in the northern SCS and ECS and weakened WS10 in the southern SCS, although the magnitudes of the simulated trends are somewhat smaller than in the reanalysis (Fig. 3b). As shown in Fig. 3c, in the northern SCS and ECS, both the ERA5 and CMIP6 multi-model ensemble mean indicates positive WS10 trends in summer, while in southern SCS both datasets reveal consistent negative WS10 trends. During winter, the ERA5 reanalysis shows that positive WS10 trends occur mainly in the northern SCS and Philippine Sea, while negative trends are observed in the southern SCS and high-latitude waters (Fig. 3d). Consistently, the CMIP6 multi-model mean has simulated an increase in WS10 over the northern SCS in winter, while WS10 decreased over the southern SCS and ECS (Fig. 3e). The simulated trends are

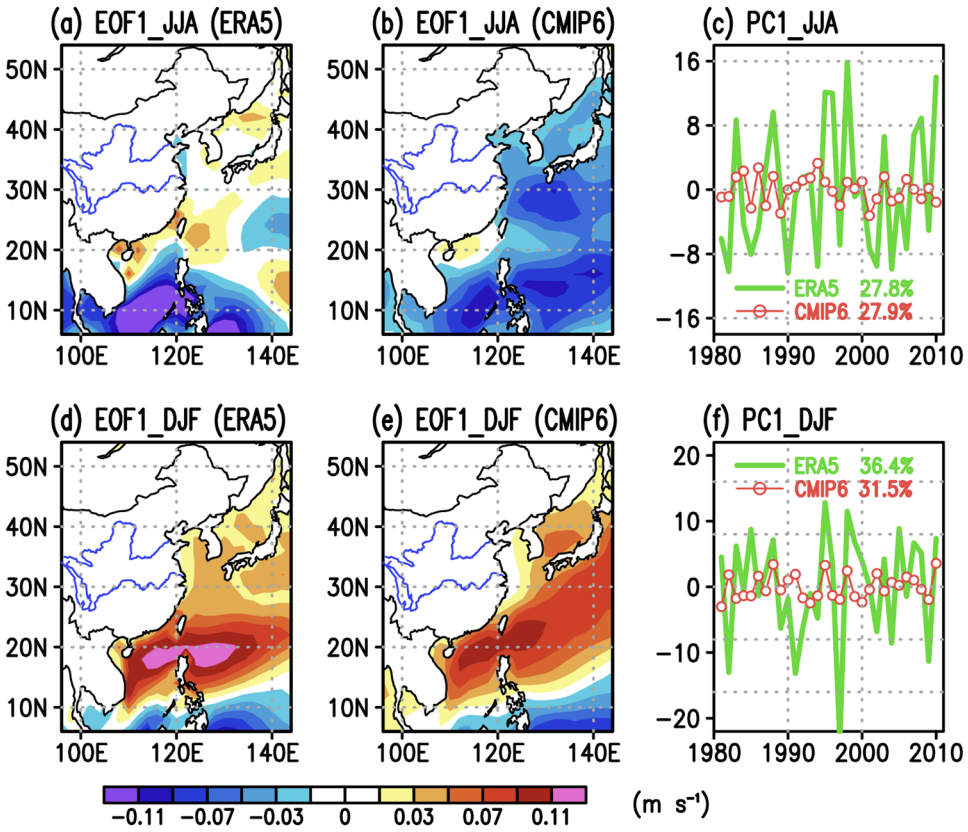

Fig. 2 Spatial patterns of the first EOF mode of WS10 variability during 1981–2010 (unit: m s^{-1}) in summer for **a** ERA5 and **b** CMIP6 multi-model ensemble mean. **c** The corresponding time series for ERA5 and CMIP6. **d**–**f** Similar to **a**–**c** except for winter

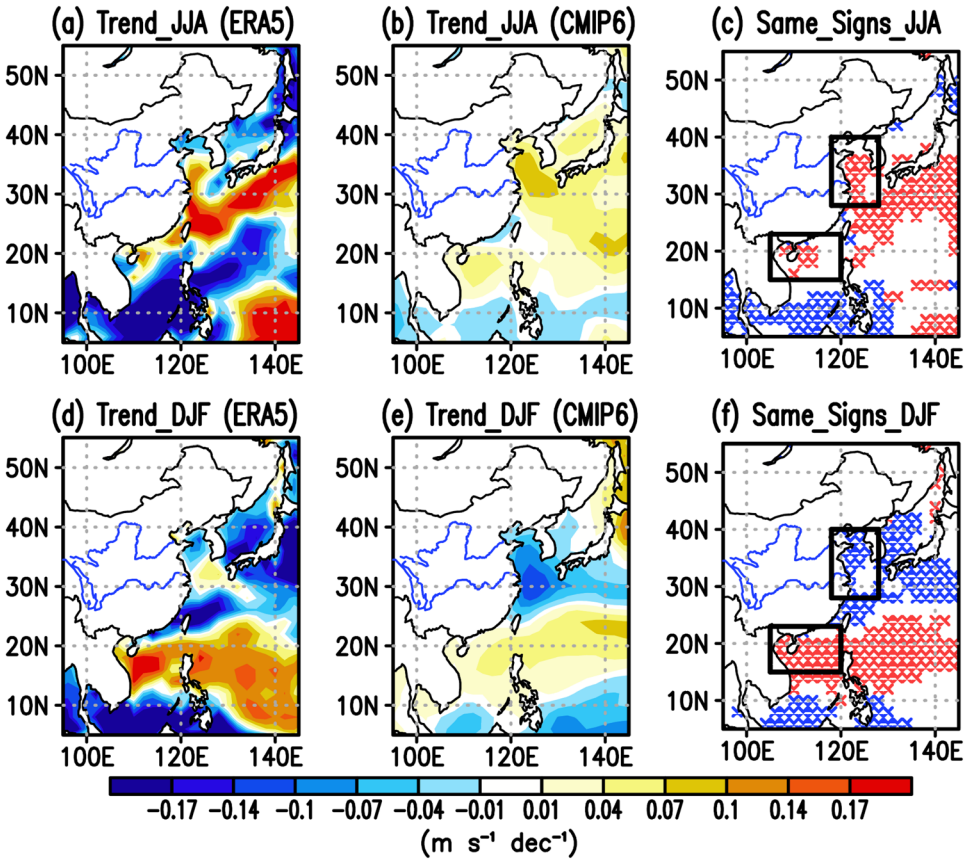

Fig. 3 The WS10 trends (1981–2010) (unit: m s^{-1} $decade^{-1}$) in summer for **a** ERA5 and **b** CMIP6 multi-model ensemble mean. **c** Areas with the same negative (blue) or positive (red) signs of the WS10 trends between ERA5 and CMIP6 are marked by the crosses. **d**–**f** Similar to **a**–**c** except for winter. The areas of the northern SCS (15°–23° N, 105°–120° E) and the ECS (28°–40° N, 118°–128° E) are roughly outlined by black rectangles

lower than those in the reanalysis, which could be because the multi-model mean could reduce the atmospheric internal variability. Moreover, as seen from Fig. 3f, the ERA5 and CMIP6 multi-model ensemble mean reveal negative WS10 trends in most areas of ECS and the Sea of Japan in winter. Meanwhile, the two datasets show consistent positive WS10 trends in the northern SCS. Therefore, in terms of the signs of the WS10 trends, the CMIP6 multi-model mean performed faithfully in simulating the WS10 changes over the coastal waters of China, especially in the northern SCS and ECS. To facilitate the assessment of the WS10 changes in the offshore seas of China, this study focuses on the northern SCS (15°–23° N, 105°–120° E) and the ECS (28°–40° N, 118°–128° E) that are outlined by black rectangles in Fig. 3c and f.

3.2 Attribution of the WS10 trends in CMIP6 historical simulations

Figure 4 shows WS10 trends in CMIP6 simulations that are individually forced by GHG, aerosols, and natural variability. In summer, the GHG-only forcing could produce increasing (decreasing) WS10 trends over the northern SCS and ECS (southern SCS), which is similar to WS10 trends in historical all-forcing simulation (Fig. 4a). Under the aerosol-only forcing, the spatial pattern of WS10 trends is opposite to the GHG-only forcing, with a decrease in WS10 over coastal China and a strengthening of WS10 over the southern SCS (Fig. 4b). Natural variability refers to the inherent variations in the Earth's climate system that occur over time due to various natural factors such as volcanic eruptions, solar radiation, and oceanic and atmospheric internal variabilities (e.g. ENSO, PDO, NAO, AMO). As shown in Fig. 4c, the natural-only forcing could result in a decreasing (increasing) WS10 trend in the coastal waters of China (southern SCS) during summer.

In winter, the responses of WS10 to the GHG and aerosol forcings are similar to those in summer, but its response to natural forcing shows distinct differences. On the one hand, the GHG-only forcing leads to increasing WS10 trends in the northern SCS, ECS, and Sea of Japan and decreasing WS10 trends in the tropical western Pacific (Fig. 4d). On the other hand, decreasing WS10 trends are forced by the aerosol-only forcing over the northern SCS and ECS (Fig. 4e), which are opposite to the GHG-only forcing in most areas. By comparison, natural variability tends to enhance the WS10 in both the northern SCS and the ECS (Fig. 4f).

As mentioned earlier, the multi-model mean of the historical CMIP6 simulation shows relatively good performance in simulating WS10 trends in the nearshore seas

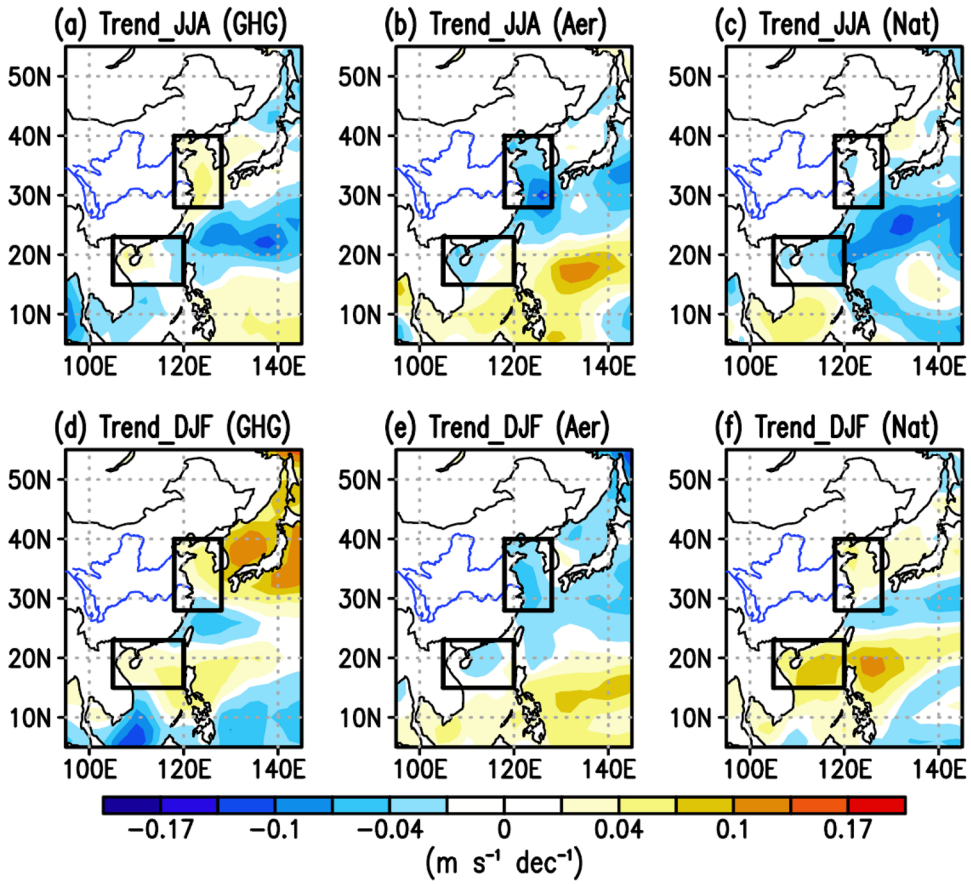

Fig. 4 The WS10 trends (1981–2010) (unit: m s^{-1} $decade^{-1}$) in summer for historical simulations individually forced by **a** greenhouse gases, **b** aerosols, and **c** natural variability. **d**–**f** Similar to **a**–**c** except for winter

of China. Therefore, we further investigate the causes of the WS10 trends, focusing on the northern SCS and ECS. As shown in Fig. 5, both the historical all-forcing and the GHG-forcing simulations show a strengthening of the WS10 trend over the northern SCS and ECS in summer. Meanwhile, both the aerosol-forcing and natural forcing simulations result in a decreasing WS10 trend over the two sea areas. In winter, the historical all-forcing simulations reproduce an increase in WS10 in the northern SCS (Fig. 4c) and a decrease in WS10 over the ECS (Fig. 4d). Similar to summer, the GHG-forcing (aerosol forcing) leads to positive (negative) WS10 trends in the two sea areas in winter. However, the natural-forcing simulations produce increasing WS10 trends in both the northern SCS and ECS in winter that are opposite to those in summer. In other words, the recent intensification of WS10 in the northern SCS and the ECS in summer can be attributed primarily to the GHG forcing. In winter, the intensification of WS10 in the northern SCS can be attributed to the GHG forcing and the effect of natural variability, while the decrease of WS10 in the ECS could be attributed to aerosol forcing.

4 Future projections of the WS10 changes in summer and winter

Figure 6 presents the future changes in summer WS10 and its zonal and meridional components projected by CMIP6 models under various SSP scenarios. As shown in the left panels, WS10 is projected to increase in the entire nearshore waters of China, with the largest increases occurring over the northern SCS and the ECS. The magnitude of the WS10 increase is more pronounced under higher SSPs. The projected changes in zonal and meridional velocities are shown in the middle and right panels. The CMIP6 models project easterly (westerly) anomalies over the southern SCS and northwestern China (the northern SCS, ECS, Sea of Japan, and the North Pacific). In addition, the models project a significant increase in meridional velocity over Chinese coastal regions and nearshore seas, including the northern SCS, ECS, and Sea of Japan. When compared to the distributions of climatological zonal and meridional velocities in summer, it can be inferred that the projected increases in WS10 over Chinese coastal regions and nearshore seas are mainly driven by the projected increases in meridional velocity, while the projected decreases in WS10 over the southern SCS are primarily caused by the projected decreases in zonal velocity.

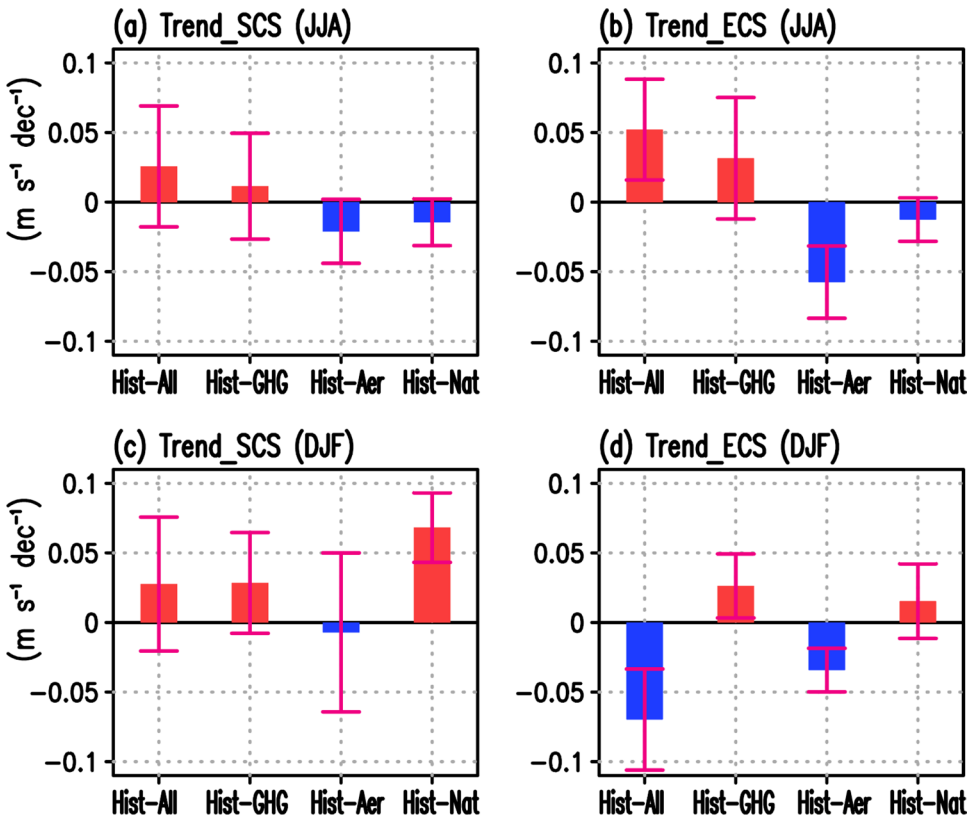

Fig. 5 The summer WS10 trends (1981–2010) (bar, unit: m s^{-1} $decade^{-1}$) and their uncertainties in CMIP6 simulations with historical all-, GHG-only, aerosol-only, and natural-only forcings for the areas of **a** northern SCS and **b** ECS. **c**, **d** Similar to **a**, **b** except for winter. The error bars represent the inter-model spreads, which indicate one standard deviation of the individual models' deviations from the mean of the 20 models

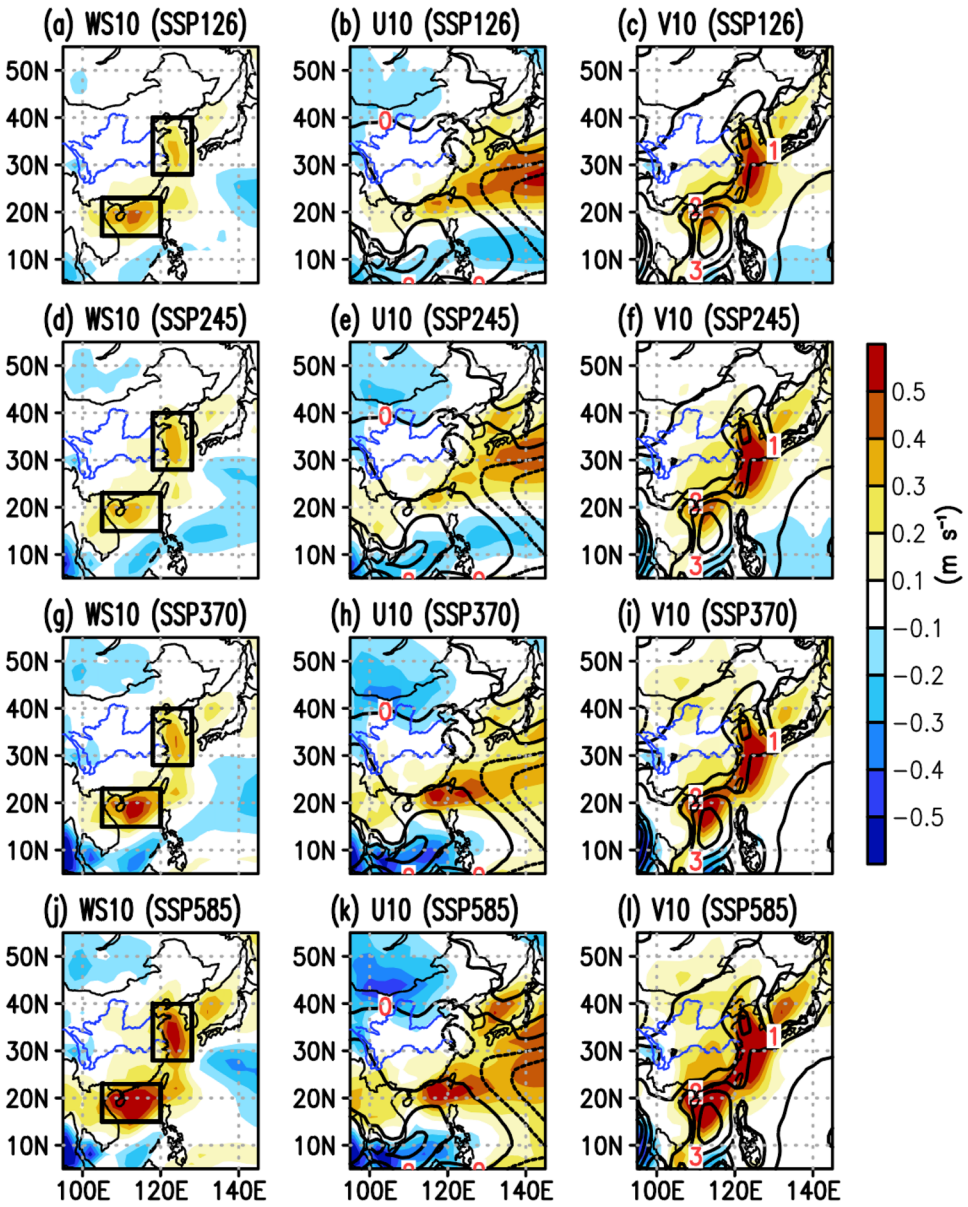

Fig. 6 Projected changes in summer WS10 (left), zonal velocity (middle), and meridional velocity (right) (average in 2070–2099 minus average in 1981–2010). The first to fourth rows correspond to the SSP126, SSP245, SSP370, and SSP585 scenarios, respectively. The contour lines in the middle and right panels indicate the climatological zonal and meridional velocities for the period 1981–2010. The black rectangles roughly outline the areas of the northern SCS (15°–23° N, 105°–120° E) and the ECS (28°–40° N, 118°–128° E)

The time series and linear trends of summer WS10 averaged over the northern SCS and the ECS, are presented in Fig. 7. In general, the summer WS10 values in the two sea areas show a robust increasing trend in the projections. Under the SSP585, by the end of the twenty-first century, WS10 is projected to increase by as much as $+0.8$ m s^{-1} ($+0.4$ m s^{-1}) over the northern SCS (ECS). For the historical period, the CMIP6 models simulated consistently increasing WS10 trends for both sea areas during summer. For the near-term and long-term future periods, under all SSP scenarios, most models project unanimous increases in WS10 over the northern SCS and the ECS.

Figure 8 presents the projected changes in winter WS10 and its zonal and meridional components. As depicted from the left panels, a projected increase in WS10 is found over the SCS, the northern Philippine Sea, and Northeast Asia, while a decrease in WS10 is projected over the southern Philippine Sea, the ECS. The projected changes in zonal and meridional velocities under various SSPs are depicted in the middle and right panels. On the one hand, easterly and northerly wind anomalies are projected over the SCS and the northern Philippine Sea, leading to an enhancement of northeasterly winds and thus an increase in the WS10 over these regions. On the other hand, westerly and southerly wind anomalies are projected over the ECS, resulting in a reduction of WS10 in this area.

Figure 9 further displays the temporal variations and linear trends of winter WS10, averaged over the northern SCS and the ECS. We see that an overall increase in WS10 exists over the northern SCS throughout the twenty-first century,

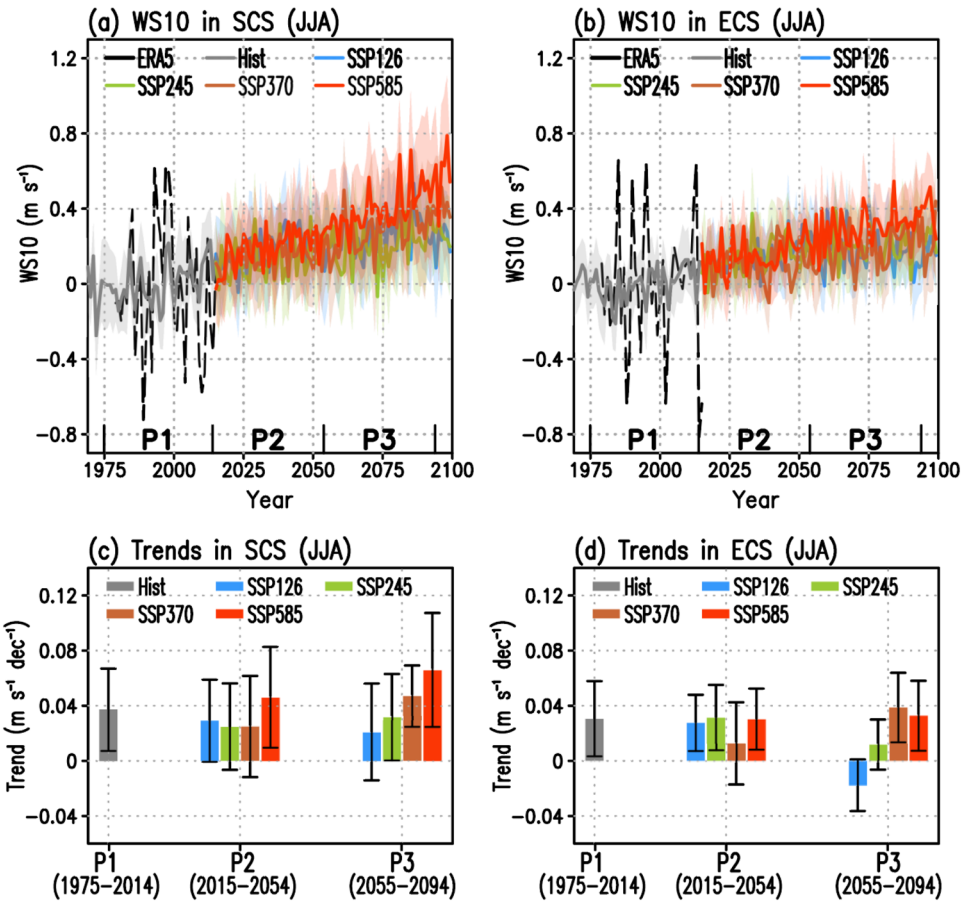

Fig. 7 **a**, **b** Time series of summer WS10 averaged over the northern SCS and ECS. The dashed lines represent data from the ERA5 reanalysis, while the grey and colored lines correspond to CMIP6 historical simulations and future projections under four different SSPs. **c**, **d** Trends in WS10 over the two regions for the historical period (P1: 1975–2014), near-term future (P2: 2015–2054), and long-term future (P3: 2055–2094). The shading in **a**, **b** and the error bars **c**, **d** represent the inter-model spreads, which indicate one standard deviation of the individual models' deviations from the mean of the twenty models

while a notable decrease in WS10 is projected in the ECS (Fig. 9a, b). The trends in WS10 for three distinct periods, namely 1975–2014, 2015–2054, and 2055–2094, are presented in Fig. 9c, d. During the historical period, the models exhibit a positive WS10 trend over the northern SCS, albeit with considerable inter-model variability. Conversely, a robust negative trend of WS10 is simulated in the ECS. For the short-term and long-term futures, the majority of models project positive WS10 trends for the northern SCS and negative trends for the ECS.

Finally, to explore the possible effects of the East Asian monsoon circulation on WS10 in the nearshore seas of China. Note that the previous studies have assessed the performance of 92 CMIP5/CMIP6 models in simulating the East Asian summer and winter monsoons, which have reported that all models can simulate the geographical distribution of the temperature and precipitation climatology and interannual variability over China reasonably well (Jiang et al. 2020). Therefore, we further examine the projected changes in the East Asian summer and winter monsoon indices in Fig. 10. In summer, the land warms faster than the water, leading to an enhanced thermal contrast between the Eurasian continent and the North Pacific Ocean. As a result, this likely leads to a stronger East Asian summer monsoon. This hypothesis is supported by most CMIP6 models, as shown in Fig. 10a, which projects a robust increase in the inversed Wang-Fan index across the four SSPs, implying an intensified monsoon circulation over East Asia and the Northwest Pacific. However, in winter, the faster warming over land could lead to a lower thermal contrast between the Eurasian continent and the Pacific Ocean. Indeed, Fig. 10b shows the consensus among most CMIP6 models, which together project a weakened WCI, implying a weakened East Asian winter monsoon circulation over various SSPs in the future. It should be noted that the projected strengthening of the East Asian summer monsoon circulation could contribute to the projected increase in WS10 over the northern SCS and ECS in summer, while the projected weakening of the East Asian winter monsoon circulation could partially explain the projected decrease in WS10 over the ECS in winter.

5 Summary and discussion

WS10 changes exert a profound influence on the natural environment and human society. This study evaluates the performance of the CMIP6 models in simulating WS10

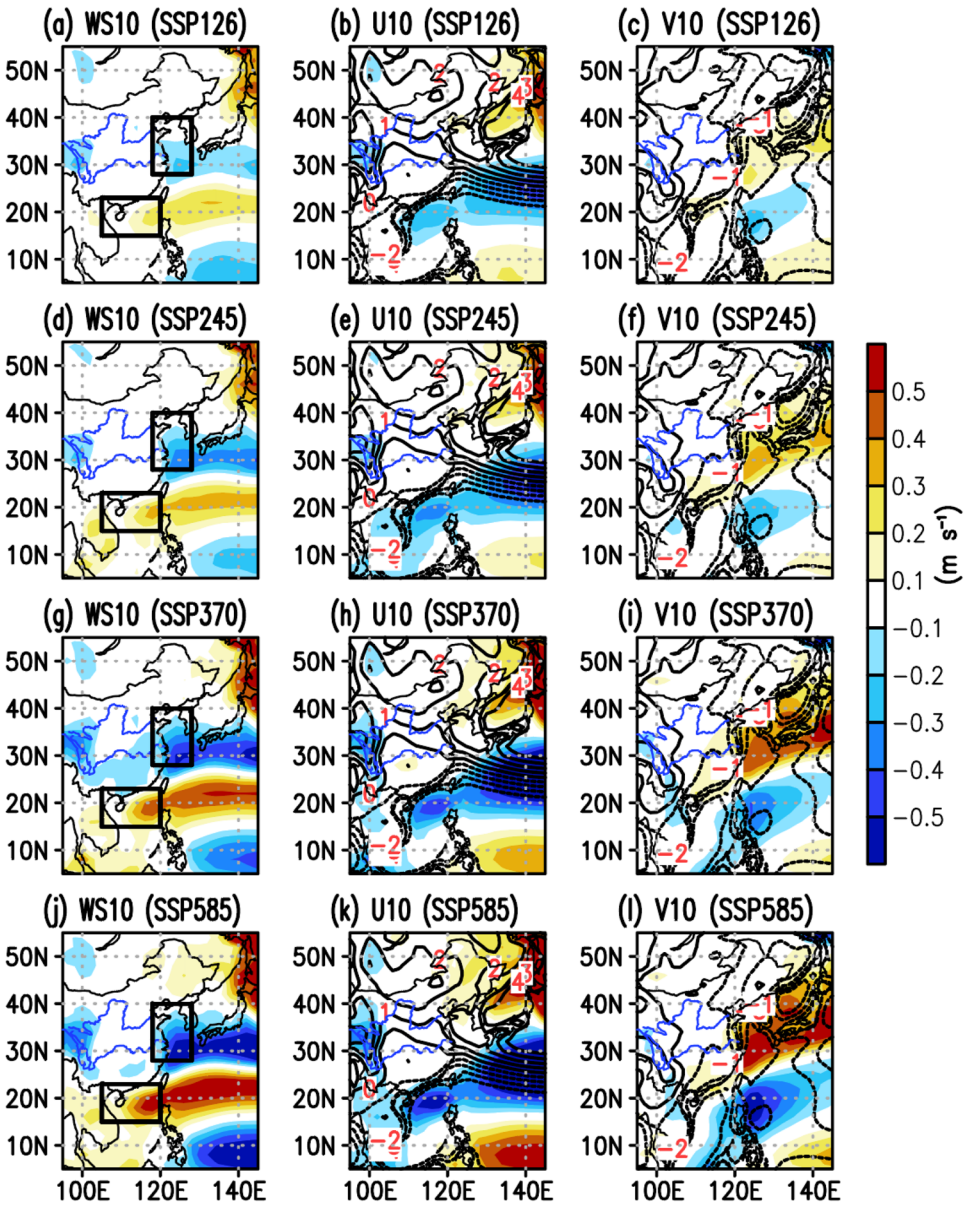

Fig. 8 Similar to Fig. 6, except for winter

changes in the summer and winter coastal waters of China. The results show that the CMIP6 models perform well in simulating climatology and performed fairly in simulating the linear trend and leading variability in WS10 over China's bordering seas. In summer, the WS10 has seen increasing trends in the northern SCS and ECS over the past several decades. However, declining tendencies were recorded in the ECS in winter WS10. Further attribution analysis shows that the recent increase in summer WS10 in the northern SCS and ECS is mainly due to the GHG forcing. During winter, the increase in WS10 in the northern SCS can be attributed to the forcing of GHG and natural variability, while the decrease in WS10 in the ECS is attributed to the aerosol forcing. Moreover, summer WS10 is projected to increase (decrease) in the northern SCS and ECS (southern SCS) in a future warming climate. By comparison, winter WS10 is projected to increase in the SCS but decrease in the ECS. Further research suggests that the projected increase in summer WS10 over the northern SCS and ECS could be caused by the projected strengthening of the East Asian summer monsoon circulation and that the projected decrease in winter WS10 over the ECS could be related to the projected weakening of the East Asian winter monsoon circulation.

This study improves our understanding of the WS10 changes in China's nearshore waters in summer and winter and their possible causes. Since changes in WS10 play a

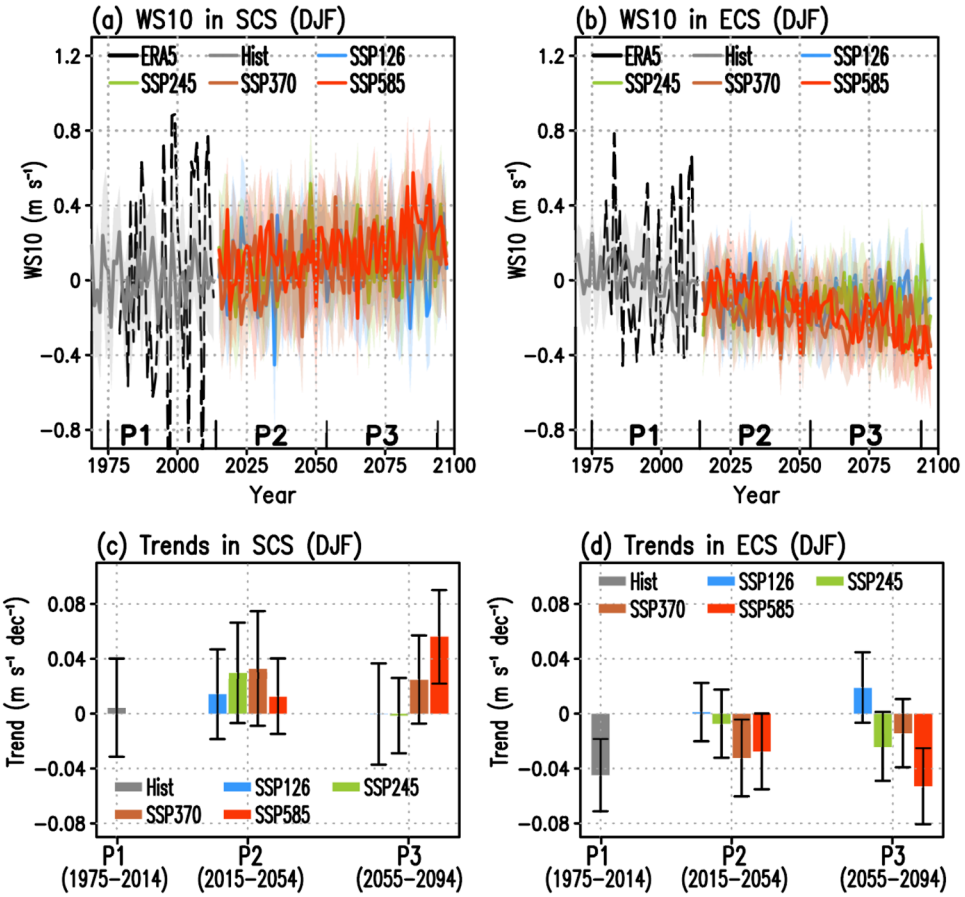

Fig. 9 Similar to Fig. 7, except for winter

key role in coastal tides and wind energy potential, a better understanding of WS10 changes can provide important insights for predicting wind-related disasters and offshore wind energy development in China. Nevertheless, it should be kept in mind that the conclusions drawn in this study were mainly derived from the ERA5 reanalysis and the CMIP6 model simulations. While the model results of this study show a satisfactory level of agreement with the reanalysis data, there are certain limitations in accurately representing WS10 in both the reanalysis data and the climate models. For example, there is a significant degree of uncertainty as to the magnitude of the WS10 trends. First, the uncertainty analysis was conducted mainly based on the ERA5 analysis. However, whether the ERA5 reanalysis data is reliable to represent the offshore winds needs to be further assessed using independent data sources (e.g. the satellite remote sensing and the buoy observations). Second, there are discrepancies between the WS10 trends from ERA5 and CMIP6 multi-model ensemble mean during the boreal summer, which reduces the reliability of the CMIP6 model simulations in this season. Moreover, in the attribution analysis, there exist large spreads of WS10 trends under the historical-all, GHG-only, and aerosol-only forcing scenarios over the northern SCS, although the multi-model ensemble mean can to some extent reduce these uncertainties. Despite these challenges, the use of reanalysis data and model simulations still offers advantages in the attribution of WS10 changes over oceanic regions. Of course, future research efforts should continue to refine and improve the simulation and prediction capabilities of the WS10 changes by incorporating more comprehensive observations over the oceans. Addressing these limitations will greatly improve the accuracy and reliability of wind disaster prediction and facilitate the planning of wind energy projects in the region.

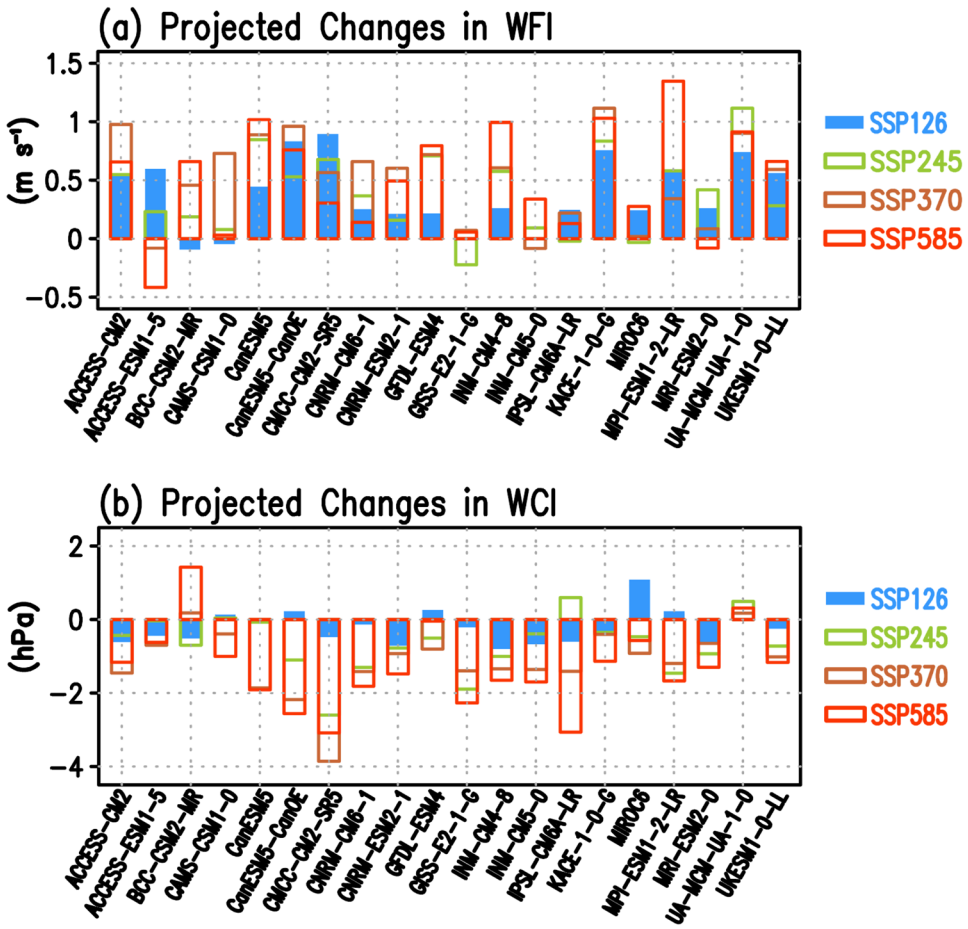

Fig. 10 Projected changes in **a** East Asian summer monsoon index (WFI; Wang and Fan 1999) and **b** East Asian winter monsoon index (WCI; Wang and Chen 2014) (average in 2070–2099 minus average in 1981–2010)

Acknowledgements We acknowledge support from the National Natural Science Foundation of China (42275020, 42230603), the Guangdong Major Project of Basic and Applied Basic Research (2020B0301030004), the Guangdong Province Key Laboratory for Climate Change and Natural Disaster Studies (2020B1212060025), and the Innovation Group Project of Southern Marine Science and Engineering Guangdong Laboratory (Zhuhai) (311021001). The author Kaiqiang Deng is also supported by the Key Laboratory of South China Sea Meteorological Disaster Prevention and Mitigation of Hainan Province (SCSF20231), the open fund of State Key Laboratory of Satellite Ocean Environment Dynamics, Second Institute of Oceanography, MNR (QNHX2310), and the Future Earth Early-Career Fellowship of the Future Earth Global Secretariat Hub China. Deliang Chen and Shen Chen are supported by Swedish STINT (CH2019-8377 and CH2020-8767).

Author contributions KD and SY contributed to the study's conception and design. Material preparation, data collection, and analysis were performed by KD. The first draft of the manuscript was written by KD. All authors commented on previous versions of the manuscript. All authors read and approved the final manuscript.

Funding This work was support by the National Natural Science Foundation of China (42275020, 42230603), the Guangdong Major Project of Basic and Applied Basic Research (2020B0301030004), the Guangdong Province Key Laboratory for Climate Change and Natural Disaster Studies (2020B1212060025), and the Innovation Group Project of Southern Marine Science and Engineering Guangdong Laboratory (Zhuhai) (311021001). The author K.D. is also supported by the Key Laboratory of South China Sea Meteorological Disaster Prevention and Mitigation of Hainan Province (SCSF20231), the open fund of State Key Laboratory of Satellite Ocean Environment Dynamics, Second Institute of Oceanography, MNR (QNHX2310), and the Future Earth Early-Career Fellowship of the Future Earth Global Secretariat Hub China. D.C. and S.C. are supported by Swedish STINT (CH2019-8377 and CH2020-8767).

Data availability The ERA5 reanalysis data is publicly available from the ECMWF website https://cds.climate.copernicus.eu/#!/search?text=ERA5&type=dataset. The simulation and projection datasets of twenty CMIP6 models are freely accessible from the portal of the Lawrence Livermore National Laboratory https://esgf-node.llnl.gov/search/cmip6/.

Declarations

Conflict of interest The authors have no relevant financial or non-financial interests to disclose.

References

Azorin-Molina C, Rehman S, Guijarro JA et al (2018) Recent trends in wind speed across Saudi Arabia, 1978–2013: a break in the stilling. Int J Climatol 38:e966–e984

Baksh AA, Abbassi R, Garaniya V et al (2018) Marine transportation risk assessment using Bayesian Network: application to Arctic waters. Ocean Eng 159:422–436

Carvalho D, Rocha A, Costoya X et al (2021) Wind energy resource over Europe under CMIP6 future climate projections: what changes from CMIP5 to CMIP6. Renew Sustain Energy Rev 151:111594

Chen H, Sun J (2013) Projected change in East Asian summer monsoon precipitation under RCP scenario. Meteorol Atmos Phys 121:55–77

Chen K, Yang S (2023) Relationships between springtime sea surface temperatures over different Indian Ocean domains and the various Asian monsoons from late spring to the following summer. J Meteorol Res 37:307–323

Chen L, Li D, Pryor SC (2013) Wind speed trends over China: quantifying the magnitude and assessing causality. Int J Climatol 33:2579–2590

Chen L, Qu X, Huang G (2019) Projections of East Asian summer monsoon under 1.5 °C and 2 °C warming goals. Theor Appl Climatol 137:2187–2201

Chen Z, Zhou T, Zhang L et al (2020) Global land monsoon precipitation changes in CMIP6 projections. Geophys Res Lett 47:e2019GL086902

Dasgupta S, Laplante B, Murray S et al (2011) Exposure of developing countries to sea-level rise and storm surges. Clim Change 106:567–579

Deng K, Azorin-Molina C, Minola L et al (2021) Global near-surface wind speed changes over the last decades revealed by reanalyses and CMIP6 model simulations. J Clim 34:2219–2234

Deng K, Liu W, Azorin-Molina C et al (2022) Terrestrial stilling projected to continue in the Northern Hemisphere mid-latitudes. Earths Future 10:e2021EF002448

Drennan WM, Graber HC, Collins CO et al (2014) EASI: an air–sea interaction buoy for high winds. J Atmos Ocean Technol 31:1397–1409

Eyring V, Bony S, Meehl GA et al (2016) Overview of the Coupled Model Intercomparison Project Phase 6 (CMIP6) experimental design and organization. Geosci Model Dev 9:1937–1958

Fan H, Hu X, Yang S et al (2021a) Process-based analysis of relative contributions to the multi-model warming projection over East Asia. Clim Dyn 56:2729–2747

Fan W, Liu Y, Chappell A et al (2021b) Evaluation of global reanalysis land surface wind speed trends to support wind energy development using in situ observations. J Appl Meteorol Clim 60:33–50

Gong H, Wang L, Zhou W et al (2018) Revisiting the northern mode of East Asian winter monsoon variation and its response to global warming. J Clim 31:9001–9014

Guo H, Xu M, Hu Q (2011) Changes in near-surface wind speed in China: 1969–2005. Int J Climatol 31:349–358

Hdidouan D, Staffell I (2017) The impact of climate change on the levelised cost of wind energy. Renew Energy 101:575–592

He C, Wang Z, Zhou T et al (2019) Enhanced latent heating over the Tibetan Plateau as a key to the enhanced East Asian summer monsoon circulation under a warming climate. J Clim 32:3373–3388

Hersbach H, Dee D (2016) ERA5 reanalysis is in production. ECMWF Newsletter 147. [Online]. http://www.ecmwf.int/sites/default/files/elibrary/2016/16299-newsletter-no147-spring-2016.pdf

Hersbach H, Bell B, Berrisford P et al (2020) The ERA5 global reanalysis. Q J R Meteorol Soc 146:1999–2049

Högström U, Rutgersson A, Sahlée E (2013) Air–sea interaction features in the Baltic Sea and at a Pacific trade-wind site: an intercomparison study. Bound Layer Meteorol 147:139–163

Huang B, Thorne PW, Banzonand VF et al (2017) Extended reconstructed sea surface temperature, version 5 (ERSSTv5): upgrades, validations, and intercomparisons. J Clim 30:8179–8205

Jiang D, Hu D, Tian Z et al (2020) Differences between CMIP6 and CMIP5 models in simulating climate over China and the East Asian monsoon. Adv Atmos Sci 37:1102–1118

Kim DY, Kim YH, Kim BS (2021) Changes in wind turbine power characteristics and annual energy production due to atmospheric stability, turbulence intensity, and wind shear. Energy 214:119051

Li Y, Yang S (2010) A dynamical index for the East Asian winter monsoon. J Clim 23:4255–4262

Li Z, Sun Y, Li T et al (2019) Future changes in East Asian summer monsoon circulation and precipitation under 1.5 to 5 °C of warming. Earths Future 7:1391–1406

Li X, Li Q, Ding Y et al (2022) Near-surface wind speed changes in eastern China during 1970–2019 winter and its possible causes. Adv Clim Change Res 13:228–239

Lin R, Zhou T, Qian Y (2014) Evaluation of global monsoon precipitation changes based on five reanalysis datasets. J Clim 27:1271–1289

Lu M, Yang S, Wang J et al (2021) Response of regional Asian summer monsoons to the effect of reduced surface albedo in different Tibetan Plateau domains in idealized model experiments. J Clim 34:7023–7036

Mariotti G, Fagherazzi S, Wiberg PL et al (2010) Influence of storm surges and sea level on shallow tidal basin erosive processes. J Geophys Res 115:C11012

McVicar TR, Roderick ML, Donohue RJ et al (2012) Global review and synthesis of trends in observed terrestrial near-surface wind speeds: implications for evaporation. J Hydrol 416–417:182–205

Miao J, Wang T (2020) Decadal variations of the East Asian winter monsoon in recent decades. Atmos Sci Lett 21:e960

Miao J, Wang T, Chen D (2020) More robust changes in the East Asian winter monsoon from 1.5 to 2.0°C global warming targets. Int J Climatol 40:4731–4749

O'Neill BC, Tebaldi C, van Vuuren DP et al (2016) The scenario model intercomparison project (ScenarioMIP) for CMIP6. Geosci Model Dev 9:3461–3482

Park J, Kim H, Wang S-Y et al (2020) Intensification of the East Asian summer monsoon lifecycle based on observation and CMIP6. Environ Res Lett 15:0940b9

Pryor SC, Barthelmie RJ, Bukovsky MS et al (2020) Climate change impacts on wind power generation. Nat Rev Earth Environ 1:627–643

Roderick ML, Rotstayn LD, Farquhar GD et al (2007) On the attribution of changing pan evaporation. Geophys Res Lett 34:L17403

Saidur R, Islam MR, Rahim NA et al (2010) A review on global wind energy policy. Renew Sustain Energy Rev 14:1744–1762

Shen C, Zha J, Li Z et al (2022) Evaluation of global terrestrial near-surface wind speed simulated by CMIP6 models and their future projections. Ann N Y Acad Sci 1518:249–263

Sun C, Xu X, Wang P et al (2022) The warming and wetting ecological environment changes over the Qinghai-Tibetan Plateau and the driving effect of the Asian summer monsoon. J Trop Meteorol 28:95–108

Vautard R, Cattiaux J, Yiou P et al (2010) Northern Hemisphere atmospheric stilling partly attributed to an increase in surface roughness. Nat Geosci 3:756–761

Wang L, Chen W (2014) An intensity index for the East Asian winter monsoon. J Clim 27:2361–2374

Wang B, Ding Q (2006) Changes in global monsoon precipitation over the past 56 years. Geophys Res Lett 33:L06711

Wang B, Fan Z (1999) Choice of South Asian summer monsoon indices. Bull Am Meteorol Soc 80:629–638

Wang B, Wu Z, Li J et al (2008) How to measure the strength of the East Asian summer monsoon? J Clim 21:4449–4463

Wen Y, Kamranzad B, Lin P (2021) Assessment of long-term offshore wind energy potential in the south and southeast coasts of China based on a 55-year dataset. Energy 224:120225

Wever N (2012) Quantifying trends in surface roughness and the effect on surface wind speed observations. J Geophys Res 117:D11104

World Forum Offshore Wind (WFO) (2023) Global Offshore Wind Report for 2022. [Online]. https://wfo-global.org/wp-content/uploads/2023/03/WFO_Global-Offshore-Wind-Report-2022.pdf. Accessed 22 Sept 2023

Wu J, Zha J, Zhao D et al (2018) Changes in terrestrial near-surface wind speed and their possible causes: an overview. Clim Dyn 51:2039–2078

Wu J, Shi Y, Xu Y (2020) Evaluation and projection of surface wind speed over China based on CMIP6 GCMs. J Geophys Res Atmos 125:e2020JD033611

Wu S, Liu J, Zhang G et al (2022) Evaluation of NCEP-CFSv2, ERA5, and CCMP wind datasets against buoy observations over Zhejiang nearshore waters. Ocean Eng 259:111832

Xin X, Wu T, Zhang J, Yao J, Fang Y (2020) Comparison of CMIP6 and CMIP5 simulations of precipitation in China and the East Asian summer monsoon. Int J Climatol 40:6423–6440

Xu M, Xu H, Ma J (2016) Responses of the East Asian winter monsoon to global warming in CMIP5 models. Int J Climatol 36:2139–2155

Xu M, Shao S, Weng N et al (2022) Analysis of optical turbulence over the South China Sea using balloon-borne microthermal data and ERA5 data. Remote Sens 14:4398

Yang Q, Li M, Zu Z et al (2021) Has the stilling of the surface wind speed ended in China? Sci China Earth Sci 64:1036–1049

Yu L (2007) Global variations in oceanic evaporation (1958–2005): the role of the changing wind speed. J Clim 20:5376–5390

Yu J, Zhou T, Jiang Z et al (2019a) Evaluation of near-surface wind speed changes during 1979 to 2011 over China based on five reanalysis datasets. Atmosphere 10:804

Yu J, Fu Y, Yu Y et al (2019b) Assessment of offshore wind characteristics and wind energy potential in Bohai Bay, China. Energies 12(15):2879

Zeng Z, Ziegler AD, Searchinger T et al (2019) A reversal in global terrestrial stilling and its implications for wind energy production. Nat Clim Change 9:979–985

Zha J, Shen C, Zhao D et al (2021) Slowdown and reversal of terrestrial near-surface wind speed and its future changes over eastern China. Environ Res Lett 16:034028

Zhang S, Li X (2021) Future projections of offshore wind energy resources in China using CMIP6 simulations and a deep learning-based downscaling method. Energy 217:119321

Zhang Z, Wang K (2020) Stilling and recovery of the surface wind speed based on observation, reanalysis, and geostrophic wind theory over China from 1960 to 2017. J Clim 33:3989–4008

Zhang Z, Wang K, Chen D et al (2019) Increase in surface friction dominates the observed surface wind speed decline during 1973–2014 in the northern hemisphere lands. J Clim 32:7421–7435

Zhang G, Azorin-Molina C, Chen D et al (2020) Variability of daily maximum wind speed across China, 1975–2016: an examination of likely causes. J Clim 33:2793–2816

Zhang G, Azorin-Molina C, Wang X et al (2022a) Rapid urbanization induced daily maximum wind speed decline in metropolitan areas: a case study in the Yangtze River Delta (China). Urban Clim 43:101147

Zhang Z, Duan K, Liu H et al (2022b) Spatio-temporal variation of precipitation in the Qinling Mountains from 1970 to 2100 based on CMIP6 data. Sustainability 14:8654

Zheng CW, Li XY, Luo X et al (2019) Projection of future global offshore wind energy resources using CMIP data. Atmos Ocean 57:134–148